A Computational and Experimental Investigation of Halloysite Silicic Surface Modifications After Alkaline Treatment

Francesco Ferrante[a,*], Marco Bertini[a], Chiara Ferlito[a], Lorenzo Lisuzzo[a], Giuseppe Lazzara[a], Dario Duca[a]

[a] *Dipartimento di Fisica e Chimica "E. Segrè", Università degli Studi di Palermo, Viale delle Scienze - 90128 Palermo, Italy*

Abstract

Density functional theory calculations were performed in order to investigate the formation of silanol groups on the outer surface of halloysite nanotubes, as possible products of the reactions with water in alkaline environments. The results, discussed in terms of energy release and structural properties of the modified surface, suggest that the formation of various kinds of silanol group constellations, and even the extraction of orthosilicic acid, are highly exothermic reaction in the presence of hydroxide ions. Thermogravimetric analysis, FT-IR, XRD and X-ray fluorescence spectrometry performed on halloysite treated at high pH conditions indicate that the adsorption of water on the outer surface occurs with higher percentage after the treatment, confirming the increased number of silanols groups.

Keywords: Clay Materials, Spiral Nanotubes, Functionalization, DFT

1. Introduction

Nanotubes are nanoparticles with a characteristic elongated, hollow structure. The first of this kind of materials, carbon nanotubes, were synthesized in 1991 and represent the best known and studied subclass. Since their discovery, hollow nanotubular structures have attracted the interest of the scientific

*Corresponding author

community, which led to the development of the inorganic counterpart of these materials consisting of nitrides, metals, metals oxides and natural clays nanotubes (Lai et al., 2010; Emanet et al., 2016; Yang et al., 2011). Among clay materials, halloysite nanotubes (Hal) belong to the family of aluminosilicates and were for the first time described by Berthier in 1826 as a dioctahedral 1:1 mineral of the kaolin group, since their chemical composition is similar to that of kaolin except for the presence of water molecules. Halloysite is structurally composed by the alternation of a Si−O tetrahedral layer overlapped to an Al−OH octahedral layer. The kaolinite-like sheet rolls up, conferring this nanoclay its peculiar tubular morphology (Lvov et al., 2016; Makó et al., 2020). The stoichiometric formula of Hal is $Al_2Si_2O_5(OH)_4 \cdot nH_2O$, which allows to distinguish the hydrated form (n=2, Hal-10Å), where a layer of water molecules is present between the inorganic layers, and the dehydrated form (n=0, Hal-7Å) obtained from Hal-10Å by moderate heating or by treatment in vacuum (Joussein, 2016). For a long time Halloysite has been of industrial interest mainly as raw material for ceramics. Since 2007, however, the tubular morphology has led to a plethora of studies where Hal is looked at as a potentially valuable nanomaterial, particularly in the design of polymeric nanocomposites, as controlled release device and as carrier for active agents to be exploited, for instance, in medicine, agriculture, environmental remediation and catalysis (White et al., 2012; Fakhrullin & Lvov, 2016; Gorrasi et al., 2014; Lisuzzo et al., 2022; Liu et al., 2016; Zsirka et al., 2016; Makaremi et al., 2015; Sadjadi et al., 2020; Zhang et al., 2019; Rozza et al., 2019). The first observation of Hal at the electron microscope showed a fibrous morphology that seemed to distinguish it clearly from the kaolinites with their typical hexagonal lamellar particles (Lvov et al., 2008; Lisuzzo et al., 2020c). By using techniques such as differential thermal analysis, infrared spectra, as well as experiments of chemical reactivity, it was possible to search for distinctive indicators (Lazzara et al., 2018). The results of these investigations reflected the interplay of water between the aluminosilicate layers of Hal and a lower structural order grade with respect to kaolinites. Natural halloysites, indeed, often contain phases of impurities and show variations in morphology

and porosity according to the different deposits from which they originate (Cavallaro et al., 2018). Commonly, Hal vary in length from the submicron scale to several microns (sometimes even greater than 3 μm), while the outer and inner diameter are in the range 30 to 190 nm and 10 to 100 nm, respectively (Pasbakhsh et al., 2013). Besides, Hal undergoes dehydration upon heating at ca. 100°C and to achieve complete removal of water molecules a treatment up to 450°C is needed. This process can lead to structural and morphological changes (Lisuzzo et al., 2020a) and is considered completely irreversible. The most important changes, however, concern heat treatments of Hal above 450°C; in fact at 500-550°C dehydroxylation occurs and at temperatures of 980-1000°C a significant exothermic event has been found corresponding to the formation of a Al_2O_3-rich phase and the complete destruction of the tubular structure. It is worth to note that Hal undergoes morphological alterations even as a result of treatment in basic or acid environment (Sidorenko et al., 2021). Following the acid treatment with H_2SO_4 (1 mol dm^{-3}) the filling of the nanotube with 10 nm diameter SiO_2 nanospheroids is observed at TEM and after several days of acid treatment there is an increase in internal diameter of the tubes, which confirms that the dissolution of Hal occurs mainly on the inner surface. On the other side, the decomposition of Hal in an alkaline medium (e.g. NaOH) leads to the release of Si(IV) into solution. The lower solubility of Al(III) compared to Si(IV) leads to its crystallization and to the formation of particles containing $Al(OH)_3$ (White et al., 2012).

In light of all these features (i.e. morphology, chemical reactivity, surface properties, high aspect ratio) and given the biocompatibily, low cost and abundant availability in nature, the use of Hal offers many advantages (Fakhrullina et al., 2015) However, the colloidal stability of Hal represents an issue that researchers need to tackle before its use both in aqueous and organic solvents (Lisuzzo et al., 2019). Similarly, achieving a good dispersion of these nanofillers in different matrices with good interactions at the interface is crucial for nanocomposites design procedures (Vahedi & Pasbakhsh, 2014). In order to overcome these limitations, the surface functionalization of Hal became com-

pelling (Yuan et al., 2008). In this context, modifications have been conducted by the reaction of different species with the hydroxyl groups on the external Si based surface of Hal (Vahedi & Pasbakhsh, 2014; Raman et al., 2013). Nonetheless, in the proper structure of Hal the external surface is covered by Si−O−Si groups, whereas −OH groups can be found only on either defective sites or at the edges of the rolling sheet. However, according to literature the pretreatement of the nanoclays in alkaline media results in the surface activation and improvement of the functionalization efficiency (Shankar et al., 2018; Wang et al., 2013a; De Silva et al., 2015).

Despite the presence of surface Si−OH groups in Hal is given for granted, very few studies were performed to systematically investigate the possible formation of silanol groups and the structures of the modified silicic layer. In particular, from the computational point of view attention has been devoted mainly to aggregation properties obtained by molecular dynamics simulations (Prishchenko et al., 2018; Pebdani & Miller, 2021), loading characteristics with respect to molecules of interest in applications (Spepi et al., 2016) and molecules adsorption on the two Hal surfaces (Ferrante et al., 2017; Rozza et al., 2019). Some recent studies report the investigation of Hal functionalization with dopants (Zhang et al., 2017) and alkoxysilane groups bearing amine-based ligands (Mehdizadeh et al., 2022) for catalytic purpose, but none of these shed any light on the formation of silanols on the outer surface. The present work aims to start filling this knowledge gap, by studying, using a density functional theory based computational approach, some likely surface configuration that can occur when Hal is treated in alkaline conditions to form silanol groups on the outer surface.

2. Models and Computation Details

All the calculations reported in the this work were performed by using the Gaussian 16 software (Frisch et al., 2016). The geometries of Hal modified structures were optimized within the Density Functional Theory (DFT) framework, by using the M06-L exchange-correlation functional (Zhao & Truhlar,

2006) together with the resolution of identity approximation for the evaluation of two-electron integrals (Eichkorn et al., 1997), which helps to reduce the computational cost for treating the large size systems here investigated. The VZP valence double-zeta plus polarization basis set of Ahlrichs and co-workers (Schaefer et al., 1992) was employed and the corresponding auxiliary functions needed for RI approximation were generated at run time. The investigation was made using a cluster approach; in particular the starting system, representing the pristine Hal surface (see Figure 1), has been tailored from a nanotube model built and investigated in our previous work through a Density Functional Tight Binding approach (Ferrante et al., 2015, 2017). The dangling bonds were saturated with hydrogen atoms and all the oxygen atoms placed at the cutting edges were kept fixed in their positions during geometry optimization, so that the Hal curvature could be maintained.

[Figure 1 about here.]

In the following, next to each figure depicting the structure of the investigated species (which will be shown in mixed ball-and-stick/wireframe representation in order to highlight the modified portion), a stylized drawing will be reported where the outer silicic surface is schematically represented by an array of hexagons. Each node point of this array is a silicon atom, the black circles are oxygen atoms on the surface or (if they are not linked on both sides) OH groups, the empty ones are oxygen atoms of the interlayer. Oxygen atoms belonging to the model edges are not displayed. The disappearing of an empty circle surrounding a crossing point means that the corresponding Si−O bond, linking the outer with the interlayer, is broken in the represented structure.

3. Materials and Methods

3.1. Materials

Halloysite, with specific surface area of 65 m^2 g^{-1} and specific gravity of 2.53 g cm^{-3}, and sodium hydroxide (NaOH, $\geq$97.0%) were purchased from Sigma-Aldrich and used without any further purification.

3.2. Alkaline modification of Halloysite

Hal (2g) were added to 40 cm^3 of a NaOH solution 4M and the dispersion was magnetically stirred for 30 minutes at 80 °C. Then, the nanoclay was separated from the aqueous phase by centrifugation at 5000 rpm for 10 min, washed three times with water to remove any excess and dried overnight at 60 °C. This sample will be referred to as alkaline Hal (aHal).

3.3. Experimental analysis

Thermogravimetric analysis (TGA) was carried out using a Q5000 IR (TA Instruments) apparatus. N_2 flow was set at 25 cm^3 min^{-1} for the sample and 10 cm^3 min^{-1} for the balance, respectively. Each sample, whose mass was ca. 5 mg, was heated from room temperature up to 800 °C with a scanning rate of 20 °C min^{-1}. The calibration was conducted on the basis of the Curie temperatures of standards (nickel, cobalt, and their alloys) (Blanco et al., 147-153). Fourier transform infrared (FTIR) measurements were performed by means of a Frontier FTIR spectrometer (PerkinElmer). The spectra were recorded at room temperature using 64 scans in the range between 4000 and 500 cm^{-1} with 2 cm^{-1} spectral resolution. The experiments were conducted on KBr pellets with a low content (<2 wt%) of milled sample. X-ray Fluorescence (XRF) spectrometry was performed using an Olympus InnovX DS-2000 Delta Standard Alloy XRF Handheld Analyzer operating in the Alloy Plus analysis mode. The X-Ray Diffraction (XRD) analysis was carried out using a Rigaku (MiniFlex) diffractometer with a copper Kα radiation source including a nickel filter. The voltage and current sources were set at 40 kV and 15 mA, respectively. The diffraction patterns were recorded from 2° to 70° with a rate of 20° min^{-1} and a step of 0.02°.

4. Results and discussion

4.1. Creation of surface silanol groups

A possible result of the reaction of silicic Hal surface with water in alkaline conditions was recently reported in our previous study (Rozza & Ferrante,

2020). Herein, the formation of two silanol groups, $-O_3SiOH$ and $-O_2Si(OH)_2$, starting from the pristine Hal outer surface, was detailed. According to DFT calculations the process was foreseen to release 467 kJ mol^{-1} of energy. It was argued that the silanol formation occurs together with the breaking of an $Si-O$ bond involving an oxygen atom from the SiO_4-AlO_6 interlayer, where a negative charge is formally left by the reaction. Since in the present work the oxygen atoms, instead of the silicon and aluminum ones (as for (Rozza & Ferrante, 2020)), were kept in frozen positions at model border, the formation energy of the $Si(OH)_2Si(OH)$ constellation on the surface, which was reoptimized, is slightly more exoergonic and equal to 482.4 kJ mol^{-1} (Figure 2); this because of the possibility for the surroundings of the charged oxygen atom to experience a slightly larger degree of relaxation. It could be legitimately hypothesized that roughly the same amount of energy would be released if the same reaction occurs in another, distant region of the already modified Hal, resulting in a nanotube surface sparsely bearing silanol groups. Therefore, it is a major aim of this work to detail instead the energetics and the geometries of regions of the surfaces which are locally dense of silanol groups, a situation that could heavily affect the functionalization (for example, through the formation of a large variety of multiple bindings with the surface).

[Figure 2 about here.]

All the investigated surface modification reactions are collected in Table 1, along with the corresponding global reaction energies. It was hypothesised that the formation of surface silanol groups could occur through the reaction of Hal with water and hydroxide ions in the ratio 1:n:m, where m can be equal to n or to n/2. The reaction product will be labeled as $Hal-Si(n,m)^{m-}$.

[Table 1 about here.]

As already suggested in reference (Rozza & Ferrante, 2020), isolated $-OH$ groups (as can occur, for example, on a zeolite surface (Ferrante et al., 2011)) cannot exist in the Hal silicic surface and that realized in $Hal-Si(1,1)^{-}$, i.e. two hydroxyl groups on a Si center and another hydroxyl on one of the nearest

silicon atom, is the minimum configuration that can be considered as a stable structure, meaning that the regular valence of all atoms of the system is satisfied (no dangling bonds are present) and there are not excessive distortions of the geometry around each atomic center. Its formation can be symbolically represented by the following reaction, where, borrowing the common usage, the (h) subscript means that the corresponding species is embedded in the nanotube.

$$\begin{aligned} &O_3SiO{-}SiO_{3\,(h)} + H_2O + OH^- \longrightarrow \\ &O_3SiOH_{(h)} + O_2Si(OH)_{2\,(h)} + O^-_{(h)} \end{aligned} \tag{1}$$

Here O^- is used to indicate the formally negatively charged oxygen framed in the interlayer. As a result of reaction (1), the hydroxyl groups of $O_2Si(OH)_2$ protrude from the surface, with the silicon atom which gained a quote of ca. 1.65 Å. A stabilizing hydrogen bond with length equal to 1.851 Å forms between the OH belonging to the two silanol groups, while another, longer hydrogen bond exists with the surrounding framework.

By following the same procedure, one can foresee possible products for the reactions of Hal with other H_2O molecules in alkaline environment. The next in the series is indeed $Hal{-}Si(2,2)^{2-}$, where the reaction (1) is applied again on the same hexagonal arrangement in the silicic surface. The formation of this species, showed in Figure 3, occurs with the release of 863.0 kJ mol^{-1} (as reported in Table 1). Being this reaction formerly the double of the previous one, a double release of energy (i.e. ca. 960 kJ mol^{-1}) could be expected as well. The fact that the reaction is less exothermic by ca. 100 kJ mol^{-1} is most likely related to the appearing of ring strains on the surrounding regions of the surface and steric hindrance between close silanol groups. In the newly formed agglomerate of silanols a geometry very similar to that of the one already present can be recognized, with one hydrogen bond of length equal to 2.074 Å. The hydrogen bond between the first group of silanols is maintained essentially unaltered and other H-bond interactions are with the surrounding oxygen atoms; it is however worth to note the new kind of hydrogen bond formed in the $Hal{-}Si(2,2)^{2-}$ system, the one between an hydroxyl group and a H atom located in the SiO_4-AlO_6 interlayer. The intervention of the interlayer atoms will acquire increasing importance as the surface will be subjected to further modifications.

[Figure 3 about here.]

A further iteration of reaction (1), indeed, leads to the formation of Hal−Si$(3,3)^{3-}$ (see Figure 4), where a number of hydrogen bonds are present with various configurations, involving the surface OH groups, the surrounding and the interlayer. Particularly interesting is the partial sharing of a proton between oxygen atoms belonging to different layers; the H center is at 1.059 Å from a surface O atom (a distance which is ca. 10% longer than the usual H-bond-forming OH average bond length in Hal according to the present calculations) and at 1.478 Å from an interlayer oxygen, which is formally negatively charged. The same issue occurs in a less pronounced way in a second H-bond configuration, with the sharing distances equal to 1.011/1.735 Å (this convention will be used throughout, where the values of distances between the shared H atom and the oxygen atoms are separated by a slash, being on the left the distance involving the O from the surface and on the right the one from the interlayer O atom). A likely consequence of this could be the migration of the negative charge from the interlayer, where it formed as a result of the Si−O bond breaking, to the outer surface.

[Figure 4 about here.]

The process where the entire Si−O hexagonal arrangement is disrupted to form three $O_3SiOH/O_2Si(OH)_2$ pairs occurs with a global release of ca. 1000 kJ mol^{-1} of energy. Thus, if the reaction started from Hal−Si$(2,2)^{2-}$, the exothermicity of the process still survive but is lowered to ca. -140 kJ mol^{-1}. This would suggest that the formation of silanol groups is not cooperative and that in mild alkaline environments the silicic Hal outer surface should preferably be sparsely populated of silanols. More locally dense arrangements of these surface groups would be achieved as the pH increases, before leaching of the silicic surface begins to occur.

A second kind of reaction that can be hypothesised on the silicic surface is represented formally by the equation

$$(O_3Si)_2O{-}SiO_{3\,(h)} + 2\,H_2O + OH^- \longrightarrow 2\,O_3SiOH_{(h)} + OSi(OH)_{3\,(h)} + O^-_{(h)} \qquad (2)$$

where two water molecules and only one OH^- comes into play. The reaction above produces a $Si(OH)_3$ group on the surface along with two SiOH moieties and the usual negative charge on a interlayer oxygen center. The simplest Hal model surface modified according to reaction (2) is the Hal$-Si(2,1)^-$ species reported in Figure 5, whose formation occurs with an energy release of ca. 700 kJ mol^{-1}. Three hydrogen bonds can be identified which interest the modified portion of the surface: the first between the SiOH and $Si(OH)_3$, the second between the latter and the surroundings and, most significant, the third H-bond which shows hydrogen sharing (with lengths 1.034/1.554 Å) between the second SiOH group and the O^- atomic center.

[Figure 5 about here.]

Applying again the reaction (2), the Hal$-Si(4,2)^{2-}$ structure is produced, characterized by two $Si(OH)_3$ and four Si(OH) groups on the surface (as showed in Figure 6). In this modified model system, whose formation would occur with the release of ca. 424 kJ mol^{-1} of energy, if calculated according to the reaction of Hal$-Si(2,1)^-$ with OH^- and two water molecules, or ca. 1120 kJ mol^{-1} with respect to the pristine Hal, a complicated network of hydrogen bonds can be identified. Some hydrogen bond interactions, particularly those localized on the $Si(OH)_3$-SiOH pair that was already present on the Hal$-Si(2,1)^-$ surface, are shorter than usual; for example, the one that had a length of 1.810 Å in Hal$-Si(2,1)^-$ is now reduced to 1.636 Å. This issue is likely due to the almost complete migration of a surface proton, the one bonded to a SiOH close to the involved portion of the surface, to the negative oxygen atom of the interlayer. This migration, with sharing lengths of 1.638/1.001 Å, causes the formal shift of the negative charge on an outer oxygen atom, which propagate its effect on the surface. In figure 6, the migrated shared H atom is enclosed in a circle.

[Figure 6 about here.]

In Hal$-Si(4,2)^{2-}$ a second partially shared hydrogen can be identified, having lengths 1.014/1.586 Å; its interlayer oxygen atom counterpart is acceptor of

another H-bond, where sharing (0.995/1.768 Å) is essentially negligible. Just this region of the Hal−Si$(4,2)^{2-}$ will be involved in another charge emersion from the interlayer, along with a strong reorganization of the whole surface, when the Hal−Si$(6,3)^{3-}$ system is considered. This species, which is schematically represented in Figure 7, is the product of the three-fold application of reaction (2) to our Hal model and the quantity of energy release accompanying its formation is ca. 276 kJ mol^{-1} if computed with respect to Hal−Si$(4,2)^{2-}$, or ca. 1395 kJ mol^{-1} when referred to the original Hal system. In the surface structure of Hal−Si$(6,3)^{3-}$ the H-bond configuration around the first $Si(OH)_3$ group returned to common values for the interaction distances and the H atom that in Hal−Si$(4,2)^{2-}$ shifted toward the interlayer is now again firmly bonded to a surface oxygen. On the other hand, hydrogen migration and charge emersion occurred on the region where the residues of the second formed $Si(OH)_3$ group lie; the sharing distances are 1.698/0.986 Å and several hydrogen atoms (one of which is partially shared, with lengths 1.006/1.599) act as donor toward the new surface oxygen atom bearing the negative charge.

[Figure 7 about here.]

The details of the surface hydrogen bonds networks (which involve the Hal interlayer to some extent) belonging to the investigated systems are not reported with the aim to characterize the structure of the modified Hal surface (not even in its modelistic form). It is clear that, for instance, three $Si(OH)_3$ groups can form on the silicic surface in a number of different ways, depending on which Si-O linkage is broken by hydrolysis; or, conversely, systems with the very same relative position of the silanol groups can show significantly different hydrogen bonds networks. As a matter of fact, it is not even sure that those presented here are the most stable configurations that can be realized when there is more than one modification on the same portion of the surface. Indeed, the simple computational evidence that, passing from Hal−Si$(4,2)^{2-}$ to Hal−Si$(6,3)^{3-}$, the surface suffers major reorganization, even in those regions not directly affected by the creation of the third $Si(OH)_3$ moiety, witnesses the high configuration

flexibility of the surface structure. Nevertheless, some recurrent phenomena can be addressed: i) the formation of the $Si(OH)_3$-SiOH pair or of the $Si(OH)_3$-2SiOH constellation by means of hydrolysis involving water in the presence of OH^- is a highly exothermic reaction, even when silanols are created in a restricted portion of the surface, and ii) the negative charge formally localized on the interlayer between the silicic and aluminic surface, and resulting from one of the Si-O bond cleavage which just binds those layers, can emerge toward the surface. It is worth to note here that these two issues are extremely important for the chemical functionalization of the Hal nanotube.

In order to make a comparison with the possible formation of silanol groups without the intervention of the hydroxide ion, as could occur at neutral pH, the products of the reactions

$$\begin{aligned} &O_3SiO{-}SiO_{3\,(h)} + 2\,H_2O \longrightarrow \\ &O_3SiOH_{(h)} + O_2Si(OH)_{2\,(h)} + OH_{(h)} \end{aligned} \tag{3}$$

were also considered. These reactions give the neutral forms of $Hal{-}Si(n,n)^{n-}$, labeled $Hal{-}Si(n,n)H$, where the interlayer oxygen atoms originated from the $Si{-}O$ bond breaking are protonated. A look at the reaction energy values reported in Table 1 reveals that reactions (3) are much less exothermic than the corresponding reactions (1). The energy difference could be likely traced back to the stabilization (by charge delocalization) of the hydroxyl group on going from vacuum to the surface, occurring on the $Hal{-}Si(n,n)^{n-}$ systems, plus contributions coming from hydrogen bonds weakening, which can be inferred by comparing H-bonds lengths in corresponding $Hal{-}Si(n,n)^{n-}$ and $Hal{-}Si(n,n)H$, and the lacking of proton sharing between oxygen atoms, both occurring in the products of surface modification involving only water. It is therefore clear that from the thermodynamic point of view alkaline conditions highly favour the formation of silanol groups on the silicic surface. The fact that the $O^-_{(h)}$ interlayer moiety is now protonated causes some changes in the hydrogen bonds network, schematically reported in Figures 8 and 9. The slight rotation of the silanol groups in the surface, originated by the presence of the interlayer OH, gives raise to elongation of the H-bonds in $Hal{-}Si(1,1)H$ and on the corresponding

portion of the other two species. The fact that hydrogen sharing cannot occur in these cases is particularly effective in Hal−Si(3, 3)H, where a large portion of the surface results substantially reorganized if compared to Hal−Si$(3,3)^{3-}$.

[Figure 8 about here.]

[Figure 9 about here.]

4.2. Extraction of Si(OH)$_4$ from the surface

As an extremization of reactions (1) and (2), the possibile products of the extraction of orthosilicic acid from the Hal model surface, potentially occuring according to the reaction

$$(\mathrm{O_3Si{-}O})_3{-}\mathrm{SiO_{(h)}} + 3\,\mathrm{H_2O} + \mathrm{OH^-} \longrightarrow 3\,\mathrm{O_3SiOH_{(h)}} + \mathrm{O^-_{(h)}} + \mathrm{Si(OH)_4} \quad (4)$$

were investigated. One application of this reaction gives rise to the Hal-Si-v$_1^-$ species and, if applied twice, to Hal-Si-v$_2^{2-}$, where one and two vacancies (v) are present on the silicic surface, respectively. The optimized structures of these two systems are reported in Figure 10a-b. The removal of Si(OH)$_4$ from the surface produces a free sites surrounded by OH groups; in both the investigated systems, these hydroxyl groups appear linked one to the other by hydrogen bonds, excepting one of them, which forms hydrogen bond with the interlayer $\mathrm{O^-}$, instead. The average distance between the oxygen atom of the OH groups overlooking the same vacancy is 2.85 Å and the Si−OH bond has almost the same length of the Si−O bond in the pristine silicic surface (an average shortening of only 0.03 Å is calculated), suggesting that the surface should not suffer large distortions due to the creation of the vacancy. This issue can be of overwhelming importance when one wants to functionalize Hal with silanol derivatives, such as $(\mathrm{EtO})_3\mathrm{Si(CH_2)_3NH_2}$ (APTES) or $(\mathrm{MeO})_3\mathrm{Si(CH_2)_3NH(CH_2)_2NH_2}$ (AEAPTMS), whose alkoxysilyl moieties can be incorporated on the surface. The Hal functionalization with this kind of molecules will be argument of future works.

The first orthosilicic acid extraction, i.e. the generation of Hal-Si-v$_1^-$, by means of water and $\mathrm{OH^-}$ in a 3 : 1 ratio is a higly exothermic reactions, releasing

ca. 650 kJ mol^{-1} of energy (Table 1), while the exothermicity of the same extraction from Hal-Si-v_1^- to form Hal-Si-v_2^{2-} is almost halved (338 kJ mol^{-1}). In this case too, therefore, the modification should preferably occur first in regions of the surface which are far away from each other, and only after that they begin to accumulate. In other words, both the formation of silanol groups and the extraction of silicic acid on/from the silicic surface do not seem to be cooperative processes.

Finally, for the sake of energetic comparison, the reaction of aluminum hydroxyde removal from the aluminic surface has been simulated by a process equivalent to reaction (4):

$$[O_2(OH)_4Al]_3{-}Al_{(h)} + 2\,H_2O + OH^- \longrightarrow$$
$$O_2(OH)_3AlOH^-_{(h)} + 2\,O_2(OH)_3AlH_2O_{(h)} + Al(OH)_3 \qquad (5)$$

Since in real halloysite systems the outer and inner surfaces are well separated by the nanotube walls (which can have the thickness of several aluminosilicate layers), we considered safe to treat the modifications potentially occurring on the silicic and aluminic surfaces by independent calculations. The species which forms by reaction by reaction 5 (its optimized geometry is showed in Figure 10c) has a vacant site on the aluminic surface of our model, which would correspond to the inner surface of Hal. It is worth to note that the reaction occurs in a completely different manner if compared to its counterpart on the silicic surface: in this case, indeed, the negative charge is already on the surface and formally localized on a OH^- coordinated to aluminum, which forms together with two water molecules, them too coordinated to Al. The energy released following the occurrence of reaction (5) is 362.1 kJ mol^{-1}, a value much smaller than the one related to the formation of Hal-Si-v_1^-, suggesting that in alkaline environment the leaching of Hal should begin from the silicic surface. These results are in good agreement with the literature. Indeed, it is reported that the treatment of Hal in a strong alkaline medium results in the partial leaching of the Si and Al atoms and in the formation of amorphous SiO_2 and $Al(OH)_3$ nanosheets (White et al., 2012).

[Figure 10 about here.]

4.3. Effect of the alkaline pretreatment

Hal nanotubes were treated with sodium hydroxide and the effects of the alkaline treatment were studied. Thermogravimetric curves for pristine Hal and alkaline Hal are reported in Figure 11, whereas the thermogravimetric parameters, *i.e.* the mass loss at 150 °C (ML_{150}), the mass residue at 800 °C (MR_{800}) and the degraded matter at 800 °C (MD_{800}), determined as (Lisuzzo et al., 2020b)

$$MD_{800} = 100 - (MR_{800} + ML_{150})$$

are reported in Table 2.

[Figure 11 about here.]

[Table 2 about here.]

It is worth to note that ML_{150}, which is related to the amount of water adsorbed at the surface of the nanoclay as moisture (Blanco & Siracusa, 2021), is different in the two samples. Namely, the values are 2.2% and 3.4% for Hal and aHal, respectively. This effect can be most likely related to the formation of hydroxyl groups on the external surface of the nanotubes due to the alkaline hydrolysis. Indeed, the silanols groups can act as active sites for the attachment of water molecules by hydrogen bonding. On the other side, the typical dehydroxylation of structural Al−OH groups can be observed between 450 and 500 °C in both samples and the mass residues at high temperature are similar each other (Duce et al., 2015).

To confirm the formation of hydroxyl groups on the surface of Hal, FTIR spectra were recorded (Figure 12). The spectra of both samples show the typical signals of halloysite. For instance, the two bands at 3695 and 3620 cm^{-1} are related to the O−H stretching vibrations of the Al_2OH groups inside the lumen of the nanotubes. Similarly, the bands of the O−H bending of water at 1638 cm^{-1}, the perpendicular Si−O stretching at ca. 1114 cm^{-1}, the in-plane Si−O stretching at ca. 1030 cm^{-1}, the deformation of inner hydroxyl groups at 911

409 cm^{-1} and the Al−O−Si deformation at 536 cm^{-1} can also be observed (Lisuzzo
410 et al., 2020c).

411 [Figure 12 about here.]

412 It is worth to note that, although the Al_2OH stretching frequencies are
413 not shifted after the alkaline treatment, the intensity of the 3695 and 3620
414 cm^{-1} bands is lower for aHal compared to the neat clay. This effect could
415 be ascribed to the partial etching of the inner alumina surface upon treatment.
416 Most importantly, a new sharper band appears at ca. 3450 cm^{-1} in the activated
417 clay, and it can be most likely related to the formation of new Si−OH groups on
418 the external surface due to the alkaline hydrolysis (Wang et al., 2013b). Overall,
419 the broaded band in the water region of FTIR spectrum of aHal compared to
420 Hal also accounts for a higher moisture content, as a consequence of the alkaline
421 activation, in agreement with the thermogravimetric results.

422 X-Ray fluorescence analysis was carried out to quantitatively evaluate the
423 effect of the alkaline pretreatment on the chemical composition of the nanoclay
424 before and after reaction with sodium hydroxide. The Si/Al ratios are 1.28
425 and 1.27 for pristine Hal and aHal, respectively, indicating that the relative
426 amounts of the two metals is not affected by the alkaline pretreatment. This
427 result can be explained by hypothesizing also a partial removal of Si species
428 from the outer surface together with the partial etching of Al species suggested
429 by FTIR analysis, thus maintaning the final Si/Al ratio constant.

430 The X-Ray Diffraction analysis was conducted to evaluate any variations on
431 the morphology of Hal. The patterns of pristine and alkaline Hal nanotubes
432 are reported in Figure 13. The untreated Hal shows its typical reflection at
433 12.0° 2θ, corresponding to the (001) basal distance of 0.73 nm. The presence
434 of this peak indicates that the clay is present in the dehydrated 7Å-form, since
435 the (001) reflection is related to the spacing between the different layers of each
436 nanotube (Barot et al., 2020). Further peaks can be observed at 20.4 and 24.5°
437 2θ, corresponding to the (020)/(110) basal spacing of 0.44 nm and (002) basal
438 spacing of 0.35 nm, respectively (Barot et al., 2020). The treatment with NaOH

has no influence on the diffraction pattern of aHal compared to Hal, being all the reflections still present in the same positions. Hence, the alkaline hydrolysis did not affect the structural properties of Hal, which maintains its peculiar hollow nanotubular morphology.

[Figure 13 about here.]

5. Conclusions

A computational investigation, based on density functional theory, is reported on the structural characteristics of silanol groups located on the outer surface of a halloysite nanotube model, as well as on the energetics of their formation, which should occur according to the reaction with water and the hydroxide ion. The results of the present study suggest that, from a thermodynamic point of view, the creation of silanols on the silicic surface is highly favoured by the alkaline environment, being the formation reaction in the presence of OH^- much more exothermic than the corresponding reaction involving only water molecules. This latter, however largely exothermic, is not to be excluded and, accordingly, silanol groups can form even at neutral conditions. Calculations show that the formation of agglomerates of silanol groups is slightly less exothermic than the formation of the same number of isolated (far away in the surface) groups which do not affect each others; this would mean that in neutral and mild alkaline environments the outer surface of Hal is sparsely disseminated of silanols, which would begin to cluster only at high pH values. The extreme reaction with water and OH^- leads to the release of $Si(OH)_4$ and the creation of holes in the outer surface; preliminary results suggest the extraction of $Al(OH)_3$ from the inner surface is a much less exothermic reaction. Both holes and protruding silanols are obviously of utmost importance for surface functionalization. Experimental analysis, which was carried out in order to support the computational findings, confirm that the silanol groups are present at higher extent after the alkaline activation of the nanoclays, as suggested by both TGA and FT-IR. Moreover, neither the composition nor the morphology of halloysite

was changed. The peculiar hollow nanotubular shape is preserved. Finally, the appearance of silanols at the outer surface of halloysite nanotubes is crucial for their improved functionalization and further use in many technological fields, such as catalysis.

Acknowledgements

This work was performed with co-financing from the European Union "FESR e FSE, PON Ricerca e Innovazione 2014-2020 - DM 1062/2021".

References

Barot, T., Rawtani, D., & Kulkarni, P. (2020). Physicochemical and biological assessment of silver nanoparticles immobilized halloysite nanotubes-based resin composite for dental applications. *Heliyon*, *6*, e03601. doi:https://doi.org/10.1016/j.heliyon.2020.e03601.

Blanco, I., Cicala, G., Latteri, A., Saccullo, G., El-Sabbagh, A. M. M., & Ziegmann, G. (147-153). Thermal characterization of a series of lignin-based polypropylene blends. *Journal of Thermal Analysis and Calorimetry*, *127*, 2017. doi:https://doi.org/10.1007/s10973-016-5596-2.

Blanco, I., & Siracusa, V. (2021). The use of thermal techniques in the characterization of bio-sourced polymers. *Materials*, *14*, 1686. doi:https://doi.org/10.3390/ma14071686.

Cavallaro, G., Chiappisi, L., Pasbakhsh, P., Gradzielski, M., & Lazzara, G. (2018). A structural comparison of halloysite nanotubes of different origin by small-angle neutron scattering (SANS) and electric birefringence. *Applied Clay Science*, *160*, 71–80. doi:https://doi.org/10.1016/j.clay.2017.12.044.

De Silva, R. T., Pasbakhsh, P., Lee, S. M., & Kit, A. Y. (2015). Zno deposited/encapsulated halloysite–poly(lactic acid) (PLA) nanocomposites for high performance packaging films with improved mechani-

cal and antimicrobial properties. *Applied Clay Science*, *111*, 10–20. doi:https://doi.org/10.1016/j.clay.2015.03.024.

Duce, C., Vecchio Ciprioti, S., Ghezzi, L., Ierardi, V., & Tinè, M. (2015). Thermal behavior study of pristine and modified halloysite nanotubes. *J. Therm. Anal. Calorim.*, *121*, 1011–1019. doi:https://doi.org/10.1007/s10973-015-4741-7.

Eichkorn, K., Weigend, F., Treutler, O., & Ahlrichs, R. (1997). Auxiliary basis sets for main row atoms and transition metals and their use to approximate coulomb potentials. *Theor. Chem. Acc.*, *97*, 119–124. doi:https://doi.org/10.1007/s002140050244.

Emanet, M., Fakhrullin, R., & Çulha, M. (2016). Boron nitride nanotubes and layer-by-layer polyelectrolyte coating for yeast cell surface engineering. *ChemNanoMat*, *2*, 426–429. doi:https://doi.org/10.1002/cnma.201600044.

Fakhrullin, R. F., & Lvov, Y. M. (2016). Halloysite clay nanotubes for tissue engineering. *Nanomedicine*, *11*, 2243–2246. doi:https://doi.org/10.2217/nnm-2016-0250.

Fakhrullina, G. I., Akhatova, F. S., Lvov, Y. M., & Fakhrullin, R. F. (2015). Toxicity of halloysite clay nanotubes in vivo: a caenorhabditis elegans study. *Environ. Sci.: Nano*, *2*, 54–59. doi:http://dx.doi.org/10.1039/C4EN00135D.

Ferrante, F., Armata, N., Cavallaro, G., & Lazzara, G. (2017). Adsorption studies of molecules on the halloysite surfaces: A computational and experimental investigation. *J Phys. Chem. C*, *121*, 2951–2958. doi:https://doi.org/10.1021/acs.jpcc.6b12876.

Ferrante, F., Armata, N., & Lazzara, G. (2015). Modeling of the halloysite spiral nanotube. *J Phys. Chem. C*, *119*, 16700–16707. doi:https://doi.org/10.1021/acs.jpcc.5b04281.

Ferrante, F., Rubino, T., & Duca, D. (2011). Butene isomerization and double-bond migration on the H-ZSM-5 outer surface: A density functional theory study. *J Phys. Chem. C*, *115*, 14862–14868. doi:10.1021/jp203284f.

Frisch, M. J., Trucks, G. W., Schlegel, H. B., Scuseria, G. E., Robb, M. A., Cheeseman, J. R., Scalmani, G., Barone, V., Petersson, G. A., Nakatsuji, H., Li, X., Caricato, M., Marenich, A. V., Bloino, J., Janesko, B. G., Gomperts, R., Mennucci, B., Hratchian, H. P., Ortiz, J. V., Izmaylov, A. F., Sonnenberg, J. L., Williams-Young, D., Ding, F., Lipparini, F., Egidi, F., Goings, J., Peng, B., Petrone, A., Henderson, T., Ranasinghe, D., Zakrzewski, V. G., Gao, J., Rega, N., Zheng, G., Liang, W., Hada, M., Ehara, M., Toyota, K., Fukuda, R., Hasegawa, J., Ishida, M., Nakajima, T., Honda, Y., Kitao, O., Nakai, H., Vreven, T., Throssell, K., Montgomery, J. A., Jr., Peralta, J. E., Ogliaro, F., Bearpark, M. J., Heyd, J. J., Brothers, E. N., Kudin, K. N., Staroverov, V. N., Keith, T. A., Kobayashi, R., Normand, J., Raghavachari, K., Rendell, A. P., Burant, J. C., Iyengar, S. S., Tomasi, J., Cossi, M., Millam, J. M., Klene, M., Adamo, C., Cammi, R., Ochterski, J. W., Martin, R. L., Morokuma, K., Farkas, O., Foresman, J. B., & Fox, D. J. (2016). Gaussian 16 Revision C.01.

Gorrasi, G., Pantani, R., Murariu, M., & Dubois, P. (2014). PLA/Halloysite nanocomposite films: Water vapor barrier properties and specific key characteristics. *Macromolecular Materials and Engineering*, *299*, 104–115. doi:https://doi.org/10.1002/mame.201200424.

Joussein, E. (2016). Chapter 2 - geology and mineralogy of nanosized tubular halloysite. In P. Yuan, A. Thill, & F. Bergaya (Eds.), *Nanosized Tubular Clay Minerals* (pp. 12–48). Elsevier volume 7 of *Developments in Clay Science*. doi:https://doi.org/10.1016/B978-0-08-100293-3.00002-9.

Lai, Y., Huang, Y., Wang, H., Huang, J., Chen, Z., & Lin, C. (2010). Selective formation of ordered arrays of octacalcium phosphate ribbons on TiO_2 nanotube surface by template-assisted elec-

trodeposition. *Colloids and Surfaces B: Biointerfaces*, *76*, 117–122. doi:https://doi.org/10.1016/j.colsurfb.2009.10.023.

Lazzara, G., Cavallaro, G., Panchal, A., Fakhrullin, R., Stavitskaya, A., Vinokurov, V., & Lvov, Y. (2018). An assembly of organic-inorganic composites using halloysite clay nanotubes. *Current Opinion in Colloid and Interface Science*, *35*, 42–50. doi:https://doi.org/10.1016/j.cocis.2018.01.002.

Lisuzzo, L., Cavallaro, G., Milioto, S., & Lazzara, G. (2020a). Effects of halloysite content on the thermo-mechanical performances of composite bioplastics. *Applied Clay Science*, *185*, 105416. doi:https://doi.org/10.1016/j.clay.2019.105416.

Lisuzzo, L., Cavallaro, G., Milioto, S., & Lazzara, G. (2020b). Halloysite nanotubes coated by chitosan for the controlled release of khellin. *Polymers*, *12*, 1766. doi:https://doi.org/10.3390/polym12081766.

Lisuzzo, L., Cavallaro, G., Milioto, S., & Lazzara, G. (2022). Pickering emulsions stabilized by halloysite nanotubes: From general aspects to technological applications. *Advanced Materials Interfaces*, *9*, 2102346. doi:https://doi.org/10.1002/admi.202102346.

Lisuzzo, L., Cavallaro, G., Parisi, F., Milioto, S., & Lazzara, G. (2019). Colloidal stability of halloysite clay nanotubes. *Ceramics International*, *45*, 2858–2865. doi:https://doi.org/10.1016/j.ceramint.2018.07.289.

Lisuzzo, L., Wicklein, B., Dico, G. L., Lazzara, G., Real, G. d., Aranda, P., & Ruiz-Hitzky, E. (2020c). Functional biohybrid materials based on halloysite, sepiolite and cellulose nanofibers for health applications. *Dalton Trans.*, *49*, 3830–3840. doi:https://doi.org/10.1039/C9DT03804C.

Liu, M., Chang, Y., Yang, J., You, Y., He, R., Chen, T., & Zhou, C. (2016). Functionalized halloysite nanotube by chitosan grafting for drug delivery of curcumin to achieve enhanced anticancer efficacy. *J. Mater. Chem. B*, *4*, 2253–2263. doi:https://doi.org/10.1039/C5TB02725J.

Lvov, Y., Wang, W., Zhang, L., & Fakhrullin, R. (2016). Halloysite clay nanotubes for loading and sustained release of functional compounds. *Advanced Materials*, *28*, 1227–1250. doi:https://doi.org/10.1002/adma.201502341.

Lvov, Y. M., Shchukin, D. G., Möhwald, H., & Price, R. R. (2008). Halloysite clay nanotubes for controlled release of protective agents. *ACS Nano*, *2*, 814–820. doi:http://dx.doi.org/10.1021/nn800259q.

Makaremi, M., De Silva, R. T., & Pasbakhsh, P. (2015). Electrospun nanofibrous membranes of polyacrylonitrile/halloysite with superior water filtration ability. *The Journal of Physical Chemistry C*, *119*, 7949–7958. doi:10.1021/acs.jpcc.5b00662.

Makó, E., Dódony, I., Pekker, P., Pósfai, M., Kovács, A., & Ható, Z. (2020). Nanoscale structural and morphological features of kaolinite nanoscrolls. *Applied Clay Science*, *198*, 105800. doi:https://doi.org/10.1016/j.clay.2020.105800.

Mehdizadeh, M., Sadjadi, S., Poater, A., Mansouri, A., & Bahri-Laleh, N. (2022). Molecular modelling aided catalyst design for pao oils hydrofinishing. *J. Mol. Liq.*, *352*, 118675. doi:https://doi.org/10.1016/j.molliq.2022.118675.

Pasbakhsh, P., Churchman, G. J., & Keeling, J. L. (2013). Characterisation of properties of various halloysites relevant to their use as nanotubes and microfibre fillers. *Applied Clay Science*, *74*, 47–57. doi:https://doi.org/10.1016/j.clay.2012.06.014.

Pebdani, M. H., & Miller, R. E. (2021). Molecular dynamics simulation of pull-out halloysite nanotube from polyurethane matrix. *Adv. Mech. Eng.*, *13*, 1–10. URL: `https://doi.org/10.1177/16878140211044663`.

Prishchenko, D. A., Zenkov, E. V., Mazurenko, V. V., Fakhrullin, R. F., Lvov, Y. M., & Mazurenko, V. G. (2018). Molecular dynamics of the halloysite nanotubes. *Phys. Chem. Chem. Phys.*, *20*, 5841–5849. doi:http://doi.org/10.1039/C7CP06575B.

Raman, V. S., Rooj, S., Das, A., Stöckelhuber, K. W., Simon, F., Nando, G. B., & Heinrich, G. (2013). Reinforcement of solution styrene butadiene rubber by silane functionalized halloysite nanotubes. *Journal of Macromolecular Science, Part A*, *50*, 1091–1106. doi:10.1080/10601325.2013.829349.

Rozza, R., Armata, N., Lazzara, G., Parisi, F., & Ferrante, F. (2019). Halloysite nanotubes and metal corrosion inhibitors: A computational and experimental study. *J. Phys. Chem. C*, *123*, 10451–10461. doi:http://dx.doi.org/10.1021/acs.jpcc.9b01641.

Rozza, R., & Ferrante, F. (2020). Computational study of water adsorption on halloysite nanotube in different pH environments. *Appl. Clay Sci.*, *190*, 105589. doi:https://doi.org/10.1016/j.clay.2020.105589.

Sadjadi, S., Koohestani, F., & Bahri-Laleh, N. (2020). Pd immobilization on the multi-amine functionalized halloysite as an efficient catalyst for hydrogenation reaction: An experimental and computational study. *Appl. Clay Sci.*, *192*, 105645. doi:https://doi.org/10.1016/j.clay.2020.105645.

Schaefer, A., Horn, H., & Ahlrichs, R. (1992). Fully optimized contracted gaussian-basis sets for atoms li to kr. *J. Chem. Phys.*, *97*, 2571–2577. doi:https://doi.org/10.1063/1.463096.

Shankar, S., Kasapis, S., & Rhim, J.-W. (2018). Alginate-based nanocomposite films reinforced with halloysite nanotubes functionalized by alkali treatment and zinc oxide nanoparticles. *International Journal of Biological Macromolecules*, *118*, 1824–1832. doi:https://doi.org/10.1016/j.ijbiomac.2018.07.026.

Sidorenko, A. Y., Kurban, Y. M., Aho, A., Ihnatovich, Z. V., Kuznetsova, T. F., Heinmaa, I., Murzin, D. Y., & Agabekov, V. E. (2021). Solvent-free synthesis of tetrahydropyran alcohols over acid-modified clays. *Molecular Catalysis*, *499*, 111306. doi:https://doi.org/10.1016/j.mcat.2020.111306.

Spepi, A., Duce, C., Pedone, A., Presti, D., Rivera, J.-G., Ierardi, V., & Tiné, M. R. (2016). Experimental and DFT characterization of halloysite nanotubes loaded with salicylic acid. *J. Phys. Chem. C*, *120*, 26759–26769. doi:https://doi.org/10.1021/acs.jpcc.6b06964.

Vahedi, V., & Pasbakhsh, P. (2014). Instrumented impact properties and fracture behaviour of epoxy/modified halloysite nanocomposites. *Polymer Testing*, *39*, 101–114. doi:https://doi.org/10.1016/j.polymertesting.2014.07.017.

Wang, Q., Zhang, J., & Wang, A. (2013a). Alkali activation of halloysite for adsorption and release of ofloxacin. *Applied Surface Science*, *287*, 54–61. doi:https://doi.org/10.1016/j.apsusc.2013.09.057.

Wang, Q., Zhang, J., & Wang, A. (2013b). Alkali activation of halloysite for adsorption and release of ofloxacin. *Appl. Surf. Sci.*, *287*, 54–61. doi:https://doi.org/10.1016/j.apsusc.2013.09.057.

White, R. D., Bavykin, D. V., & Walsh, F. C. (2012). The stability of halloysite nanotubes in acidic and alkaline aqueous suspensions. *Nanotechnology*, *23*, 065705. doi:https://doi.org/10.1088/0957-4484/23/6/065705.

Yang, G., Yang, X., Yang, C., & Yang, Y. (2011). A reagentless amperometric immunosensor for human chorionic gonadotrophin based on a gold nanotube arrays electrode. *Colloids and Surfaces A: Physicochemical and Engineering Aspects*, *389*, 195–200. doi:https://doi.org/10.1016/j.colsurfa.2011.08.027.

Yuan, P., Southon, P. D., Liu, Z., Green, M. E. R., Hook, J. M., Antill, S. J., & Kepert, C. J. (2008). Functionalization of halloysite clay nanotubes by grafting with γ-aminopropyltriethoxysilane. *J. Phys. Chem. C*, *112*, 15742–15751. doi:https://doi.org/10.1021/jp805657t.

Zhang, H., Cheng, C., Song, H., Bai, L., Cheng, Y., Ba, X., & Wu, Y. (2019). A facile one-step grafting of polyphosphonium onto halloysite nanotubes initiated by Ce(IV). *Chem. Commun.*, *55*, 1040–1043. doi:http://dx.doi.org/10.1039/C8CC08667B.

Zhang, Y., Fu, L., Shu, Z., Yang, H., Tang, A., & Jiang, T. (2017). Substitutional doping for aluminosilicate mineral and superior water splitting performance. *Nanoscale Res. Lett.*, *12*, 456. doi:https://doi.org/10.1186/s11671-017-2192-8.

Zhao, Y., & Truhlar, D. G. (2006). A new local density functional for main-group thermochemistry, transition metal bonding, thermochemical kinetics, and noncovalent interactions. *J. Chem. Phys.*, *125*, 194101. doi:https://doi.org/10.1063/1.2370993.

Zsirka, B., Horvath, E., Szabó, P., Yuzakova, T., Szilagyi, R., Fertig, D., Makó, E., Varga, T., Kónya, Z., Kukovecz, A., & Kristóf, J. (2016). Thin-walled nanoscrolls by multi-step intercalation from tubular halloysite-10 Å and its rearrangement upon peroxide treatment. *Applied Surface Science*, *399*, 245. doi:https://doi.org/10.1016/j.apsusc.2016.12.053.

List of Figures

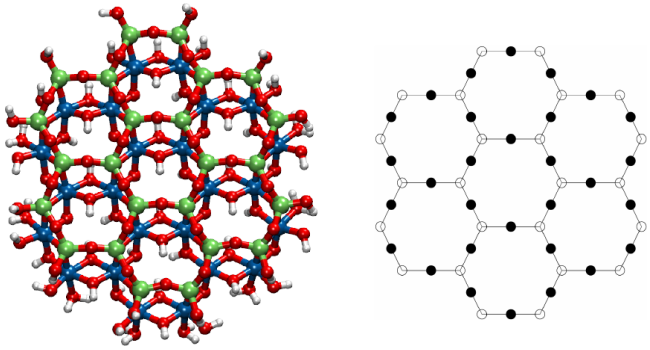

Figure 1: The Hal model employed in this work, along with the schematic representation of the silicic surface which will be used throughout. Here the black dots are oxygen atoms of the surface; at each crossing point there is a silicon atom, forming the fourth bond with the interlayer oxygen located below, represented by a transparent circle.

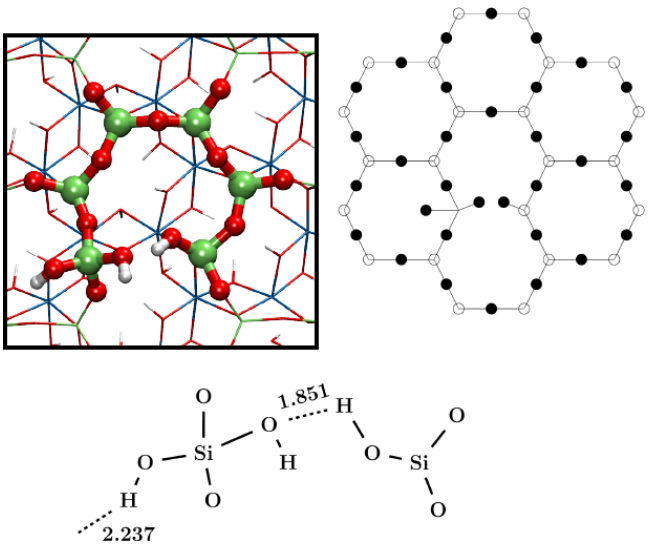

Figure 2: The portion of the optimized geometry of Hal−Si$(1,1)^{-}$ relevant to the present investigation is shown in the frame, on the right of which there is a schematic representation of the bond breaking occurring on the silicic surface, accompanying the formation of the silanol groups. The hydrogen bonds present on the modified surface are depicted on the bottom. The dashed lines with no ending symbol indicate interactions with atomic centers in the surrounding Hal frame; the hydrogen bonds lengths, in Å, are reported close to the interaction lines.

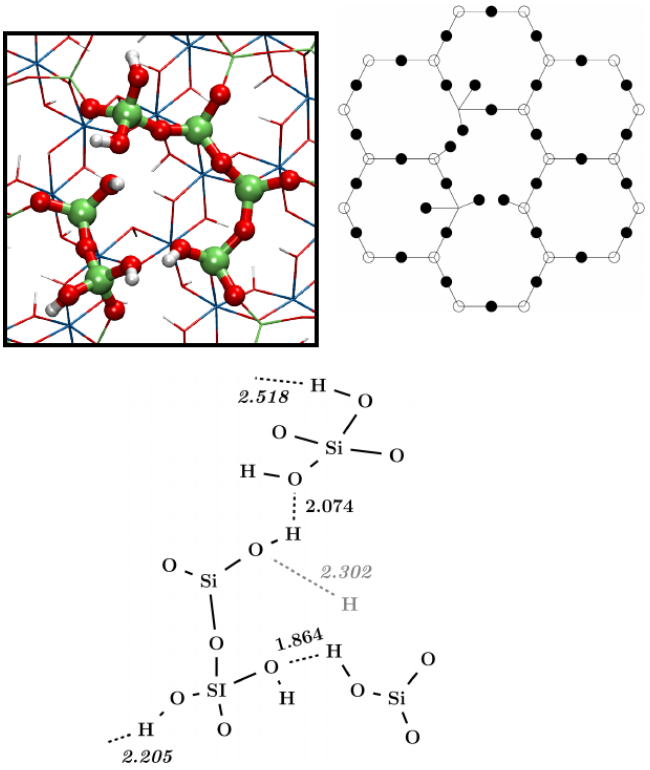

Figure 3: The relevant portion of the optimized geometry of Hal−Si$(2,2)^{2-}$, the bond breaking scheme and the surface hydrogen bonds network. Here, the length of hydrogen bonds, in Å, are reported close to the dashed lines; the lines with no ending atoms and length values in italic indicate interactions with the surrounding Hal frame while those in grey color correspond to H-bond interactions with the interlayer atomic centers.

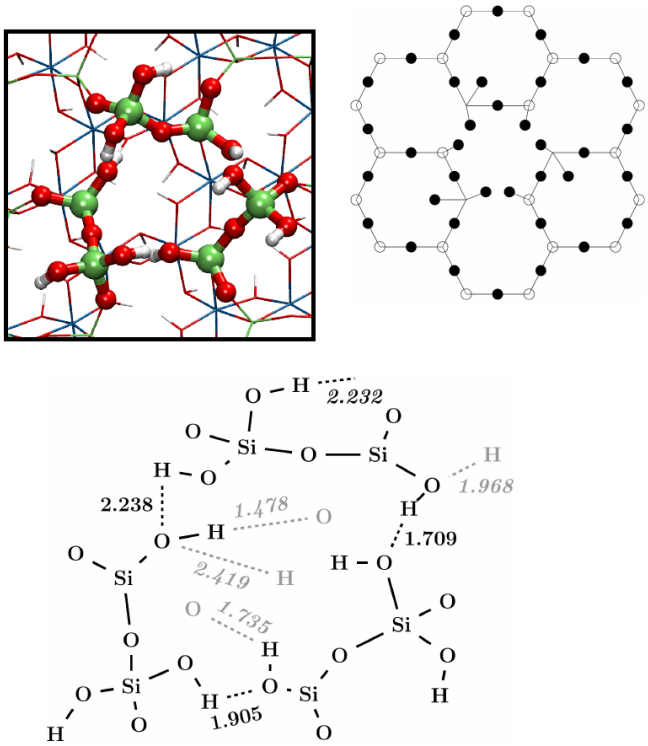

Figure 4: The relevant portion of the optimized geometry of Hal−Si(3, 3)$^{3-}$, along with the scheme of silanol groups formation and the hydrogen bonds network present in the involved region of the silicic surface.

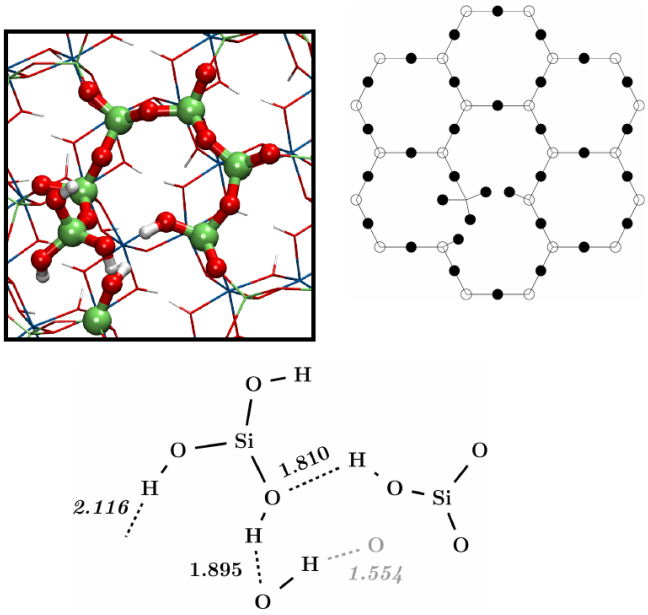

Figure 5: Framed is the portion of the optimized geometry of the Hal−Si$(2,1)^{-}$ system showing the result of one application of reaction (2) on the silicic surface. The bond breaking scheme and the hydrogen bonds network are reported on the right and below, respectively.

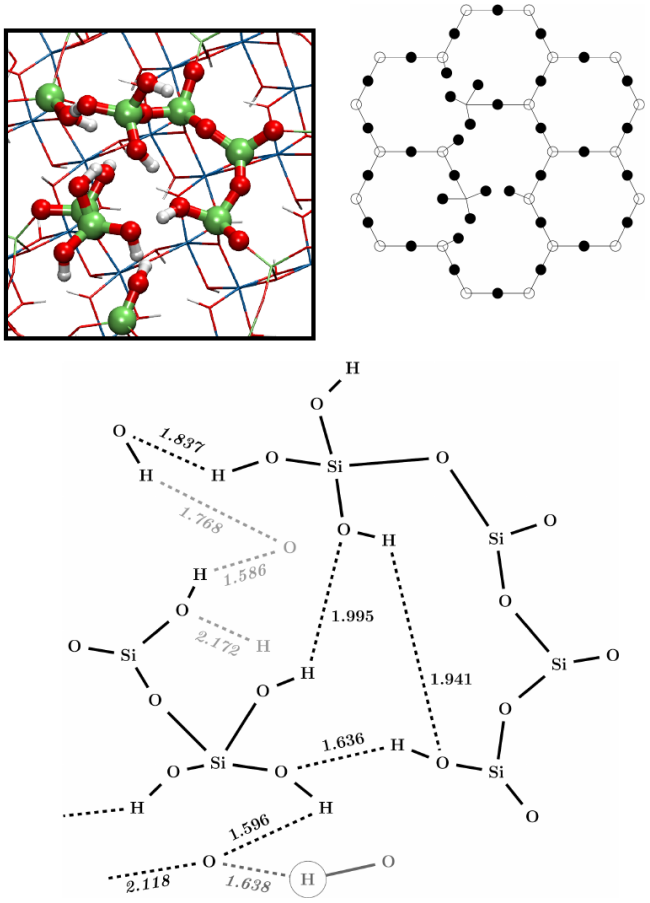

Figure 6: The optimized geometry of Hal−Si$(4,2)^{2-}$, along with the bond breaking scheme and the description of the hydrogen bonds network. The H atom, which shifted from the interlayer to the silicic surface, is the one enclosed in the circle.

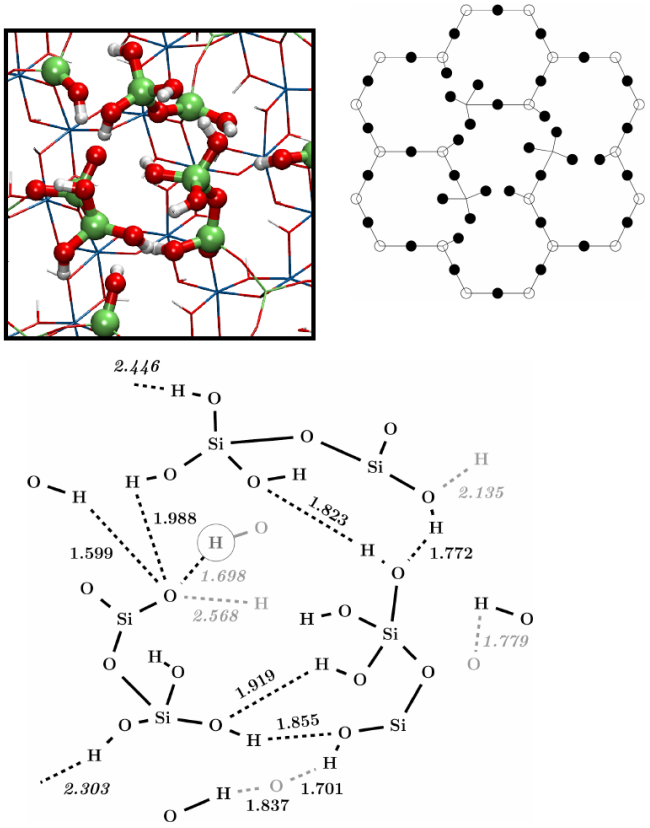

Figure 7: The optimized geometry of Hal−Si$(6,3)^{3-}$. The circle around the H atom indicates that the atom is shared between two oxygen centers.

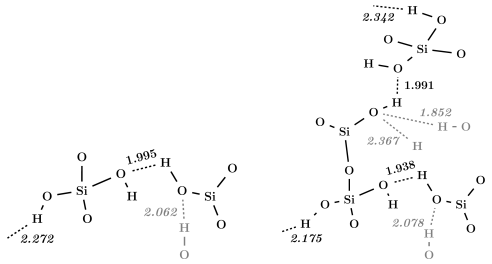

Figure 8: Schematic representation of the hydrogen bonds network occurring in Hal−Si(1, 1)H (left) and Hal−Si(2, 2)H (right). The O−H groups emphasized in pale grey are the protonated form of the $O^{-}_{(h)}$ species.

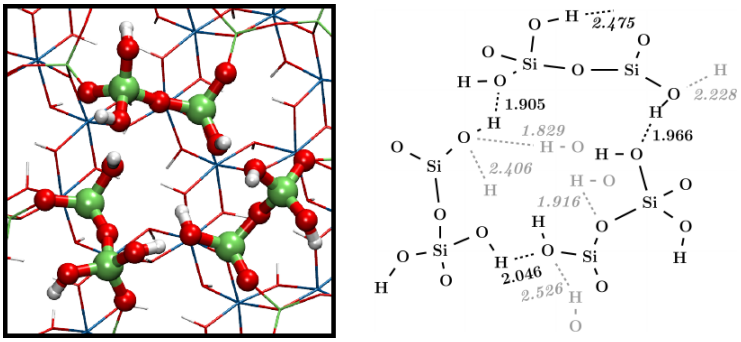

Figure 9: The optimized geometry of Hal−Si(3, 3)H with the schematic representation of its hydrogen bonds network. The O−H groups emphasized in pale grey are the protonated form of the $O^{-}_{(h)}$ species.

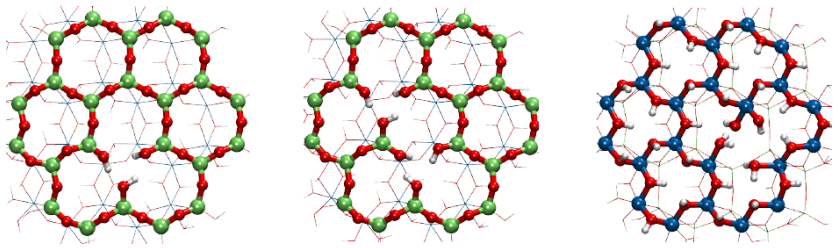

(a) **(b)** **(c)**

Figure 10: The optimized geometries of (a) Hal-Si-v_1^-, (b) Hal-Si-v_2^{2-} and (c) the system showing a vacancy on the aluminic surface, originated by the application of reaction (4) on the silicic surface and of reaction (5) on the aluminic one, respectively.

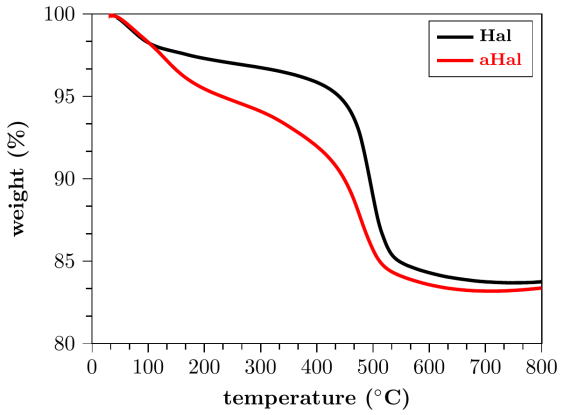

Figure 11: Thermogravimetric curves of pristine and alkaline Hal.

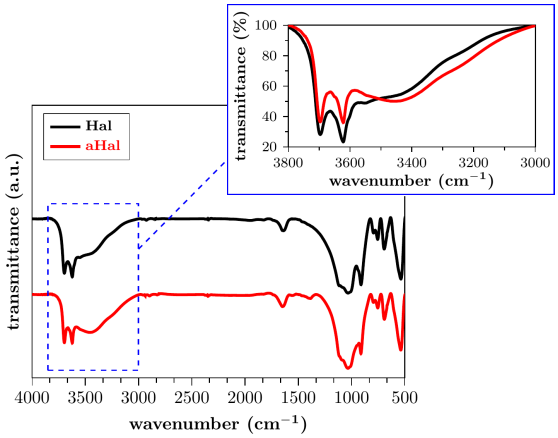

Figure 12: FTIR spectra of pristine and alkaline Hal. The FTIR spectra in the 3800-3000 cm^{-1} range are reported enlarged in the inset.

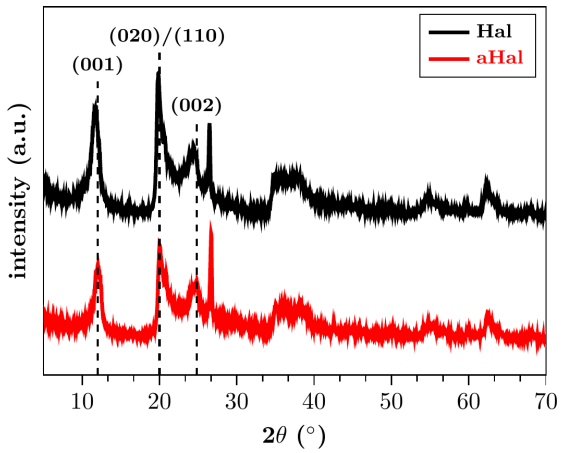

Figure 13: Diffractograms of pristine and alkaline Hal.

List of Tables

Table 1: Reactions energies (kJ mol^{-1}) for the processes investigated in this work, regarding the formation of silanol groups on the silicic surface and the removal of silicic acid.

Surface modification in alkaline conditions	
$\mathrm{Hal} + \mathrm{H_2O} + \mathrm{OH^-} \longrightarrow \mathrm{Hal{-}Si(1,1)^-}$	-482.4
$\mathrm{Hal} + 2\,\mathrm{H_2O} + 2\,\mathrm{OH^-} \longrightarrow \mathrm{Hal{-}Si(2,2)^{2-}}$	-863.0
$\mathrm{Hal} + 3\,\mathrm{H_2O} + 3\,\mathrm{OH^-} \longrightarrow \mathrm{Hal{-}Si(3,3)^{3-}}$	-1002.6
$\mathrm{Hal} + 2\,\mathrm{H_2O} + \mathrm{OH^-} \longrightarrow \mathrm{Hal{-}Si(2,1)^-}$	-696.4
$\mathrm{Hal} + 4\,\mathrm{H_2O} + 2\,\mathrm{OH^-} \longrightarrow \mathrm{Hal{-}Si(4,2)^{2-}}$	-1119.9
$\mathrm{Hal} + 6\,\mathrm{H_2O} + 3\,\mathrm{OH^-} \longrightarrow \mathrm{Hal{-}Si(6,3)^{3-}}$	-1395.4
Surface modification in neutral conditions	
$\mathrm{Hal} + 2\,\mathrm{H_2O} \longrightarrow \mathrm{Hal{-}Si(1,1)H}$	-236.2
$\mathrm{Hal} + 4\,\mathrm{H_2O} \longrightarrow \mathrm{Hal{-}Si(2,2)H}$	-308.3
$\mathrm{Hal} + 6\,\mathrm{H_2O} \longrightarrow \mathrm{Hal{-}Si(3,3)H}$	-403.7
Extraction from the surface	
$\mathrm{Hal} + 3\,\mathrm{H_2O} + \mathrm{OH^-} \longrightarrow \mathrm{Hal{-}Si{-}v_1^-} + \mathrm{Si(OH)_4}$	-650.4
$\mathrm{Hal} + 6\,\mathrm{H_2O} + 2\,\mathrm{OH^-} \longrightarrow \mathrm{Hal{-}Si{-}v_2^{2-}} + 2\,\mathrm{Si(OH)_4}$	-988.3

Table 2: Thermogravimetric parameters of pristine and alkaline Hal.

sample	$\mathbf{ML_{150}(wt\%)}$	$\mathbf{MR_{800}(wt\%)}$	$\mathbf{MD_{800}(wt\%)}$
Hal	2.2	83.8	10.0
aHal	3.4	83.4	13.2